Submitted to the
XXII International Symposium on Lepton-Photon Interactions at High Energy
30 June - 5 July, Uppsala, Sweden

Abstract: 261 **Session:EW&B,QCD/HS**

Measurement of neutral current deep inelastic scattering at high Bjorken-x

ZEUS Collaboration

Abstract

A new method is employed to measure the neutral current cross section up to Bjorken-x values equal to one with the ZEUS detector at HERA using an integrated luminosity of 65.1 pb^{-1} for e^+p collisions and of 16.7 pb^{-1} for e^-p collisions. Cross sections have been extracted for $Q^2 > 576\ \text{GeV}^2$ and are compared to predictions using different parton density functions. The data produce new constraints on the form of the parton density functions at the highest values of x.

1 Introduction

At HERA, proton beams of 920 GeV (820 GeV prior to 1998), collide with either electron or positron beams of 27.5 GeV. The electron[1] interacts with the proton via the exchange of a gauge boson. The exchanged boson can be a neutral particle (photon or Z^0), leading to a so-called Neutral Current (NC) interaction, or an electrically charged W, leading to a Charged Current (CC) interaction.

The description of deep inelastic scattering (DIS) is usually given in terms of three Lorentz invariant quantities, Q^2, x and y, which are related by $Q^2 = sxy$, the masses of the electron and proton are neglected, and where s is the square of the center-of-mass energy. The electron-proton differential scattering cross section is typically written in terms of the proton structure functions as

$$\frac{d^2\sigma}{dxdQ^2} = \frac{2\pi\alpha^2}{xQ^4}\left[(1+(1-y)^2)F_2(x,Q^2) \pm (1-(1-y)^2)xF_3(x,Q^2)\right]$$

where the contribution from F_L has been neglected. The contribution from xF_3 is positive for electron beams and negative for positron beams.

The structure functions F_2 and xF_3 can be written in terms of parton distribution functions (PDFs) and electroweak parameters. The PDFs are found to decrease very quickly for $x \geq 0.3$. The form of the PDFs is typically parametrized as $(1-x)^\eta$ as $x \to 1$, as expected from counting rule arguments [1], and this form follows the data quite well [2,3]. However, a direct confrontation with data has not been possible to date for $x \to 1$ due to limitations in beam energies and measurement techniques. The highest measured points in the DIS regime are for $x = 0.75$ [4]. Data at higher x exist [5, 6] but these are in the resonance production region and cannot be easily interpreted in terms of parton distributions. The highest x value for HERA structure function data is $x = 0.65$. In this paper, new measurements are reported from the ZEUS collaboration on differential cross sections extending to $x = 1$ for $Q^2 \geq 576$ GeV^2.

2 Experimental setup and new reconstruction method

ZEUS is a multipurpose detector described in detail elsewhere [7]. A schematic depiction of the ZEUS detector is given in Fig. 1. The components most relevant in this analysis are the uranium–scintillator calorimeter (CAL) [8], which consists of three parts: the forward

[1] In the following, we use the term electron to represent both electrons and positrons unless specifically noted otherwise.

(FCAL), the barrel (BCAL) and the rear (RCAL) calorimeters, and the central tracking detector (CTD) [9].

The measurements are based on the data collected by ZEUS from 1998 to 2000. The data correspond to an integrated luminosity of 65.1 pb^{-1} for e^+p collisions and 16.7 pb^{-1} for e^-p collisions at $\sqrt{s} = 318$ GeV.

Figure 1 includes a schematic depiction of a NC event: a scattered electron and a jet are outlined in the CAL, while the proton remnant largely disappears down the forward beam pipe. E'_e and E_{jet} are the energies of the scattered electron and jet; θ_e and θ_{jet} are the polar angles with respect to the proton beam direction. As x increases, the jet is boosted in the forward direction and θ_{jet} decreases. When x is too high, a part of the jet is lost in the beam pipe. The value of x at which this occurs is Q^2 dependent: the x value for which jets are well contained increases as Q^2 increases. At the Q^2 values considered in this analysis, the scattered electron is at large angles and well contained in the detector.

The new method employed in this analysis combines electron and jet information to allow a measurement of the differential cross section up to $x = 1$. Events are first sorted into Q^2 bins using information from the electron only: $Q^2 = 2E_eE'_e(1 + \cos\theta_e)$, where E_e is the electron beam energy. The jet information is then used to calculate x from E_{jet} and θ_{jet} for events with a well recontructed jet. These events are sorted into x bins to allow a measurement of the double differential cross section $d^2\sigma/dxdQ^2$. Events with no jet reconstructed within the fiducial volume are assumed to come from high x and are collected in a bin with $x_{Edge} < x < 1$. Since these bins are generally large and the form of the PDF is not well known in this region, an integrated cross section is calculated; $\int_{x_{Edge}}^{1}(d^2\sigma/dxdQ^2)dx$. Events with more than one high energy jet are discarded.

The features of this method are:

- good resolution in Q^2 for all x;
- good resolution in x in events where a jet can be reconstructed;
- cross section measurements possible up to $x = 1$.

3 Data selection and comparison to simulations

The following criteria were imposed to select appropriate DIS events:

- a scattered electron in BCAL or FCAL with $E'_e \geq 25$ GeV to ensure high electron-finding efficiency and negligible backgrounds. Tight fiducial cuts were placed on the electron to ensure high measurement resolution. Additionally, the energy in a cone around the electron, E_{CONE}, was required to be less than 4 GeV, to ensure isolation of the scattered electron;

- for the Z component of the vertex $|Z_{vtx}| < 50$ cm was required to remove background events from non-ep interactions;
- if the electron was in the CTD acceptance, a track was required, which, when extrapolated to the CAL, yielded a distance of closest approach (DCA) < 10 cm.

The following cuts were used to select good jets:

- 0 or 1 jet found using k_T clustering algorithm [10] with $E_T^{jet} > 10$ GeV and $\theta_{jet} > 0.12$ rad. Events with multiple reconstructed jets satisfying these requirements were rejected.

The following kinematic cuts were used to select an essentially background free and well reconstructed event sample:

- $40 < E - p_Z < 70$ GeV to remove events with large initial-state radiation, where the longitudinal energy-momentum variable $E - p_Z$ is calculated using the energy deposits and angles measured with the CAL. The lower cut value is 47 GeV for events in the highest x bins;
- $y_e < 0.95$ to remove events with fake electron candidates from photoproduction background which are found in the FCAL, where y_e is y calculated from electron method;
- $p_T/\sqrt{E_T} < 4\ \sqrt{\text{GeV}}$ to remove events from cosmic rays and beam-related background.

Standard Model (SM) NC events were simulated using the HERACLES 4.6.1 [11] program with the DJANGOH version 1.1 [12] interface to the hadronization programs. Corrections for the initial and final-state electroweak radiation, vertex and propagator corrections, and two-boson exchange are included. The hadronic final state was simulated using the MEPS model of LEPTO 6.5 [13], which includes order-α_S matrix elements and models of higher-order QCD radiation. The color-dipole model in ARIADNE 4.08 [14] provided a systematic check. The CTEQ4D PDFs set [15] was used to evaluate the nominal Standard Model (SM) cross section.

Generated events were input into a GEANT 3.13-based simulation [16] of the ZEUS detector. Trigger and offline processing requirements as used for the data were applied to the simulated events.

The simulated MC events were used to evaluate the efficiency for the event selection and to determine the accuracy of the kinematic reconstruction. A sufficient number of events was used to ensure the statistical uncertainties from the MC samples were negligible compared to those in the data.

MC distributions are compared with those from the data of both e^+p and e^-p collisions for several variables as described below. The MC distributions have been normalized to the measured luminosity. The comparison to e^+p data is shown. The comparison of e^-p data with MC distributions showed similar features. The first set of plots, Fig. 2, shows general properties for the full sample of events. Good agreement between data and MC simulation is observed, and there is no indication of residual backgrounds. Figure 3 shows distributions related to the scattered electron. Figure 4 presents a series of control plots for jet quantities. The MC reproduces the data distribution for the number of reconstructed jets to high accuracy. This is important since the MC is used to correct for the inefficiency resulting from the requirement of exactly zero or one reconstructed jets. The remaining distributions in this figure are for the jet quantities in one jet events. Figure 5 shows distributions for the class of events with zero jets. Overall, 10 % more data events for e^+p and 6 % more data events for e^-p are observed for zero jet events than expected in the simulation. An offset in the $E - p_Z$ distribution is seen, with the MC distribution slightly lower than the data, but generally the distributions agree well and there is no indication of background in the sample.

The bin definitions used in this analysis are given in Fig. 6. The bin widths for the double differential cross section measurements were chosen to correspond to three times the resolution of the reconstructed kinematic variables. The x resolution of the new method is better than that of the double angle (DA) method [17, 18] which is usually used by ZEUS, which allows a more accurate measurement and smaller bins as shown in the figure. The bin structure ZEUS published [19] is also shown. In total, 16 Q^2 bins were chosen with central values ranging from $Q^2 = 576\,\mathrm{GeV}^2$ to $Q^2 = 5253\,\mathrm{GeV}^2$. The definition of the x bin boundaries vary with Q^2 since x_{Edge} is strongly Q^2 dependent, with typically 6 x bins defined for each Q^2 bin.

The MC simulation was used to study the x distribution of the zero jet events which are assigned to the highest x bin. Figure 7 shows the true x distribution for the e^+p MC events in different Q^2 bins. Similar distributions are observed in the e^-p MC. As can be seen in this figure, the zero jet events originate predominantly from the interval $x_{Edge} < x < 1$. The purity in these bins is high and comparable to the purity in mid-x bins.

4 Results and conclusion

The measured Born level cross sections for e^+p and e^-p are shown in Fig. 8 and Fig. 9 and compared to SM expectations at NLO using the CTEQ6D PDFs [20]. The predictions for the highest x bins only change by less than 5% when switching from CTEQ4D to CTEQ6D PDFs and even less for low x bins. The double differential cross sections are represented by solid points, and generally agree well with the expectations. The cross section in the highest x bin is given as

$$\frac{1}{1-x_{Edge}} \int\limits_{x_{Edge}}^{1} \frac{d^2\sigma}{dxdQ^2} dx \quad .$$

In this bin, the expected cross section is drawn as a horizontal line, while the measured cross section is displayed as the open symbol. The measured data is plotted at the center of the bin, but it should be understood to be an integrated cross section for the bin. The error bars represent the quadratic sum of the systematic and statistical uncertainties. The systematic uncertainties are dominated by the jet energy scale uncertainty (2 %), the jet angle reconstruction, and the simulation of the hadronic final state. Typical systematic uncertainties range from 0.5% to 3%.

The ratios of the measured cross sections to Standard Model expectation using the CTEQ6D PDFs for e^+p and e^-p are shown in Fig. 10 and Fig. 11. The ratio of the expectation using the CTEQ6D PDFs to that using ZEUS-S PDFs [21] is also shown. The measured double differential cross sections generally agree well with both sets of expectations. For the highest x bins, which are in previously unmeasured kinematic ranges, the data has a tendency to lie above the expectations. These data are expected to have an impact on the extraction of the PDFs at the highest values of x, and via sum rules, also the PDFs at smaller x.

References

[1] S. Brodsky and G.Farrar, Phys. Rev. Lett. **31**, 1153 (1973).

[2] A.D. Martin et al., Preprint hep-ph/0201127, 2002.

[3] J. Pumplin et al., Preprint hep-ph/0201195, 2002.

[4] BCDMS Coll., A.C. Benvenuti et al., Phys. Lett. **B 223**, 485 (1989).

[5] L.W. Whitlow et al., Phys. Lett. **B 282**, 475 (1992).

[6] M.Osipenko et al., Phys. Rev. **D 67**, 092001 (2003).

[7] ZEUS Coll., U. Holm (ed.), *The ZEUS Detector*. Status Report (unpublished), DESY (1993), available on `http://www-zeus.desy.de/bluebook/bluebook.html`.

[8] M. Derrick et al., Nucl. Inst. Meth. **A 309**, 77 (1991);
A. Andresen et al., Nucl. Inst. Meth. **A 309**, 101 (1991);
A. Caldwell et al., Nucl. Inst. Meth. **A 321**, 356 (1992);
A. Bernstein et al., Nucl. Inst. Meth. **A 336**, 23 (1993).

[9] N. Harnew et al., Nucl. Inst. Meth. **A 279**, 290 (1989);
B. Foster et al., Nucl. Phys. Proc. Suppl. **B 32**, 181 (1993);
B. Foster et al., Nucl. Inst. Meth. **A 338**, 254 (1994).

[10] S. Catani et al., NP **B**, 187 (1993).

[11] A. Kwiatkowski, H. Spiesberger and H.-J. Möhring, Comp. Phys. Comm. **69**, 155 (1992). Also in *Proc. Workshop Physics at HERA*, 1991, DESY, Hamburg.

[12] G.A. Schuler and H. Spiesberger, *Proc. Workshop on Physics at HERA*, W. Buchmüller and G. Ingelman (eds.), Vol. 3, p. 1419. Hamburg, Germany, DESY (1991);
H. Spiesberger, HERACLES *and* DJANGOH*: Event Generation for ep Interactions at HERA Including Radiative Processes*, 1998, available on
`http://www.desy.de/~hspiesb/djangoh.html`.

[13] G. Ingelman, A. Edin and J. Rathsman, Comp. Phys. Comm. **101**, 108 (1997).

[14] L. Lönnblad, Comp. Phys. Comm. **71**, 15 (1992).

[15] CTEQ Coll., H.L. Lai et al., Eur. Phys. J. **C 12**, 375 (2000).

[16] R. Brun et al., GEANT3, Technical Report CERN-DD/EE/84-1, CERN, 1987.

[17] S. Bentvelsen, J. Engelen and P. Kooijman, *Proc. Workshop on Physics at HERA*, W. Buchmüller and G. Ingelman (eds.), Vol. 1, p. 23. Hamburg, Germany, DESY (1992).

[18] K.C. Höger, *Proc. Workshop on Physics at HERA*, W. Buchmüller and G. Ingelman (eds.), Vol. 1, p. 43. Hamburg, Germany, DESY (1992).

[19] ZEUS Coll., S. Chekanov et al., Phys. Rev. **D 70**, 052001 (2003).

[20] J. Pumplin, et al., JHEP **0207**, 012 (2002).

[21] ZEUS Coll., S. Chekanov et al., Phys. Rev. **D 67**, 12007 (2003).

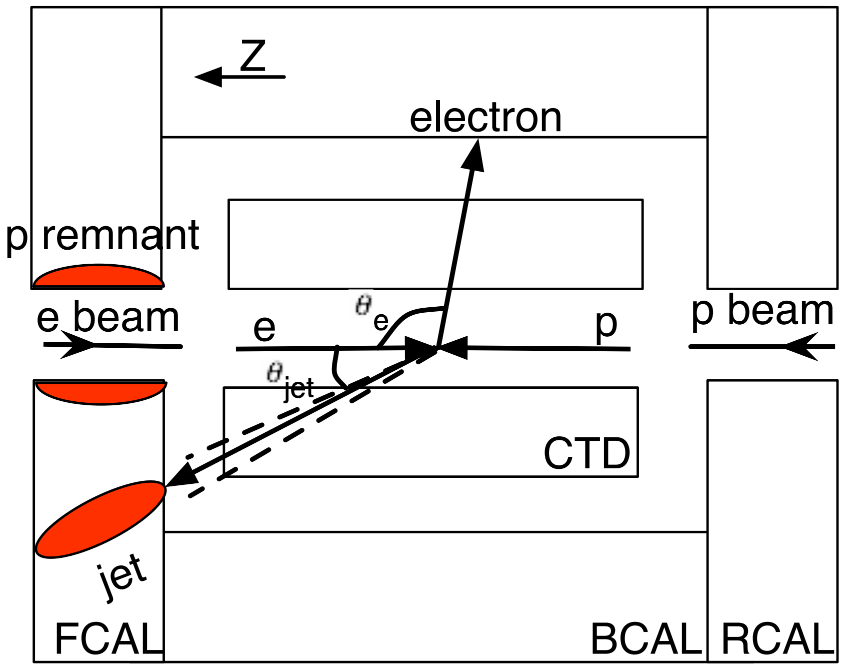

Figure 1: *A schematic depiction of the ZEUS detector with the main components used in this analysis labeled. Also shown is a typical topology for events studied in this analysis. The electron is scattered at large angles and is reconstructed using the central tracking detector (CTD) and the barrel calorimeter (BCAL), while the scattered jet is typically reconstructed in the forward calorimeter (FCAL). The jet of particles from the proton remnant largely disappears down the beam pipe.*

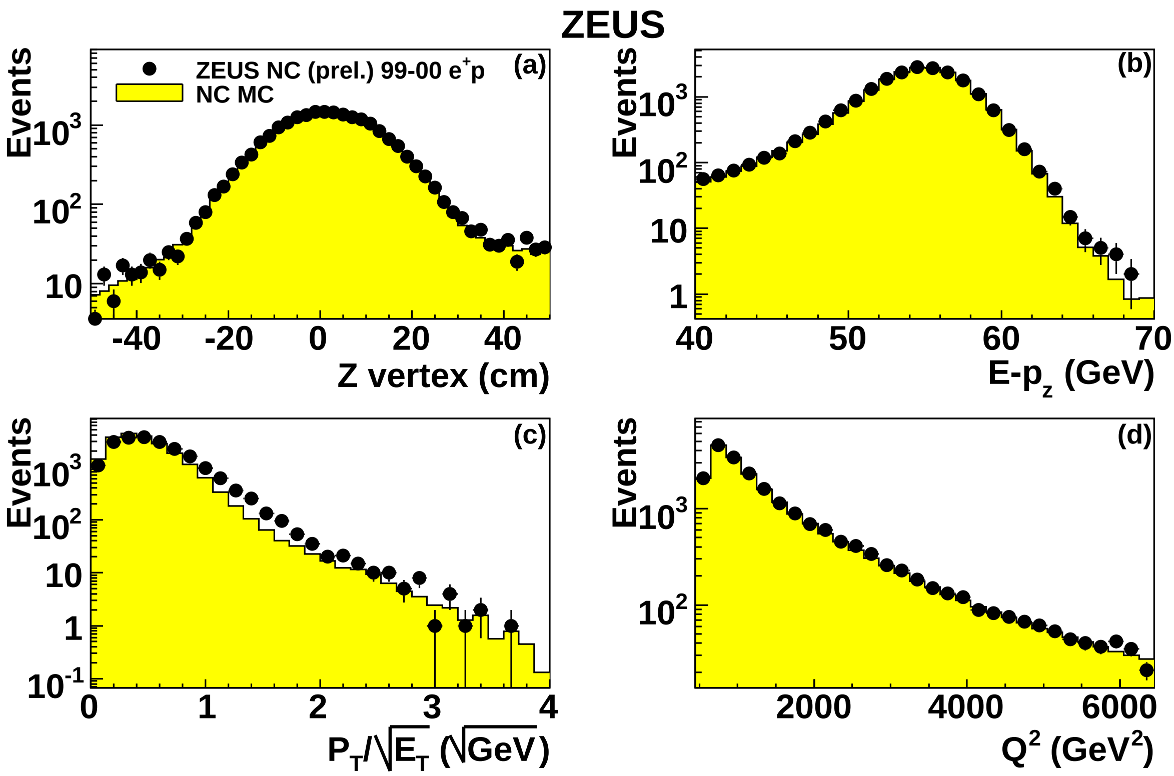

Figure 2: *Comparison of NC MC simulated events (histograms) with data (points) for: (a) the Z coordinate of the events vertex; (b) $E - p_z$; (c) $P_T/\sqrt{E_T}$ and (d) Q^2. The MC distributions are normalized to the luminosity of the data. Only e^+p data are shown in Figs 2-7.*

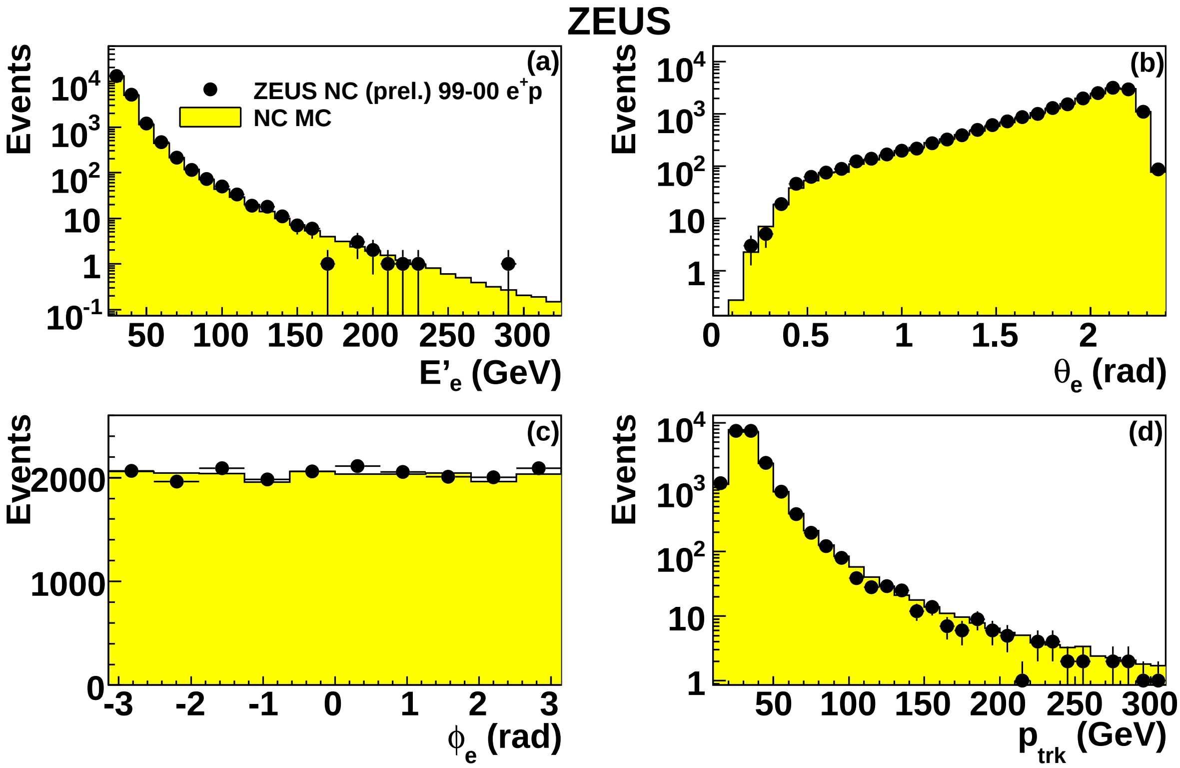

Figure 3: *Comparison of NC MC distributions (histograms) with data (points) for: (a) E'_e; (b) θ_e; (c) ϕ_e and (d) P_{trk}, the momentum of the track associated with the scattered electron. The MC distributions are normalized to the luminosity of the data.*

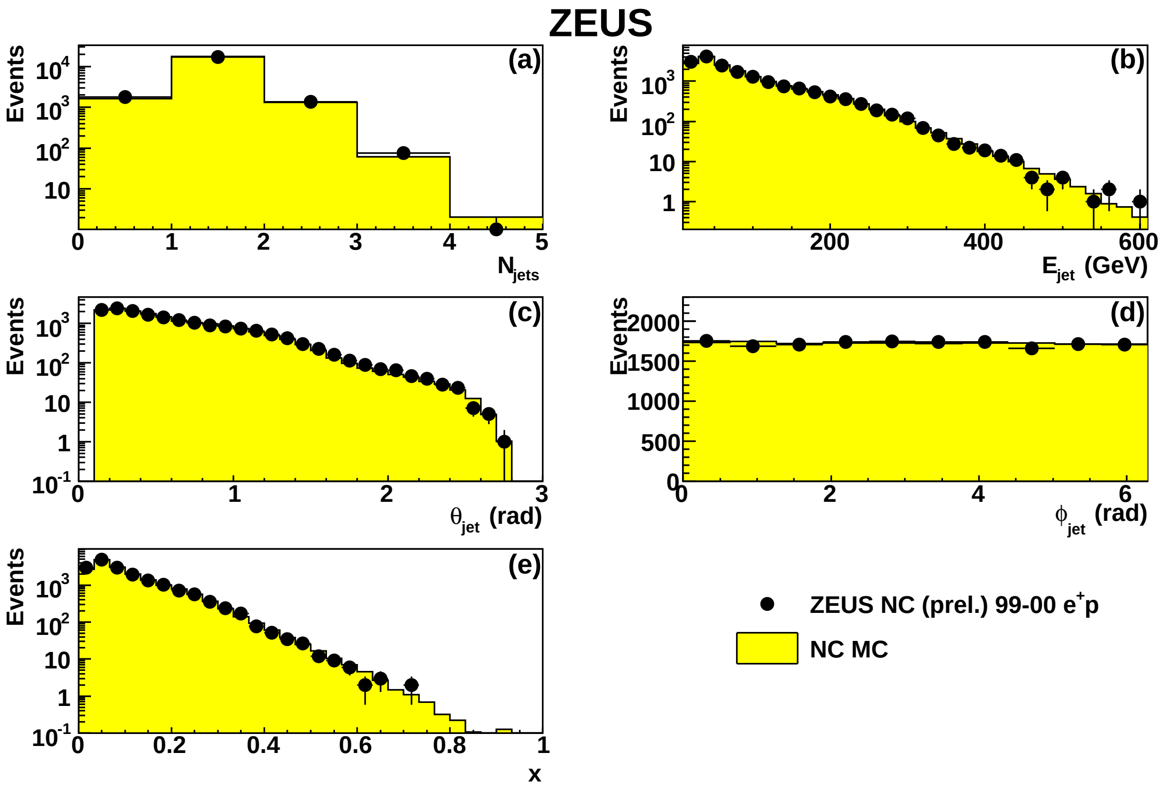

Figure 4: *Comparison of NC MC distributions (histograms) with data (points) for: (a) the number of reconstructed jets; (b) E_{jet}; (c) θ_{jet}; (d) ϕ_{jet} and (e) x calculated from the jet. The jet distributions are for one jet events. The MC distributions are normalized to the luminosity of the data.*

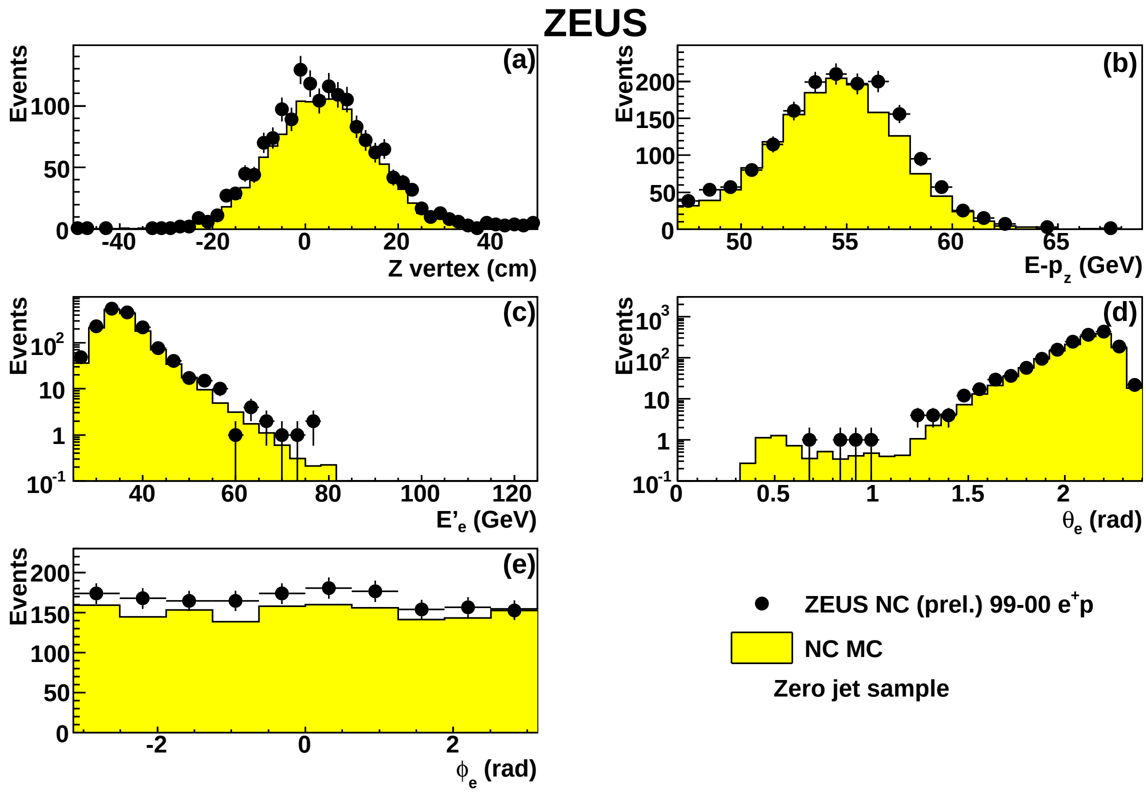

Figure 5: *Comparison of NC MC distributions (histograms) with data (points) for events with zero jets. The plots show: (a) the Z coordinate of the events vertex; (b) $E - p_z$; (c) E'_e; (d) θ_e and (e) ϕ_e. The MC distributions are normalized to the luminosity of the data.*

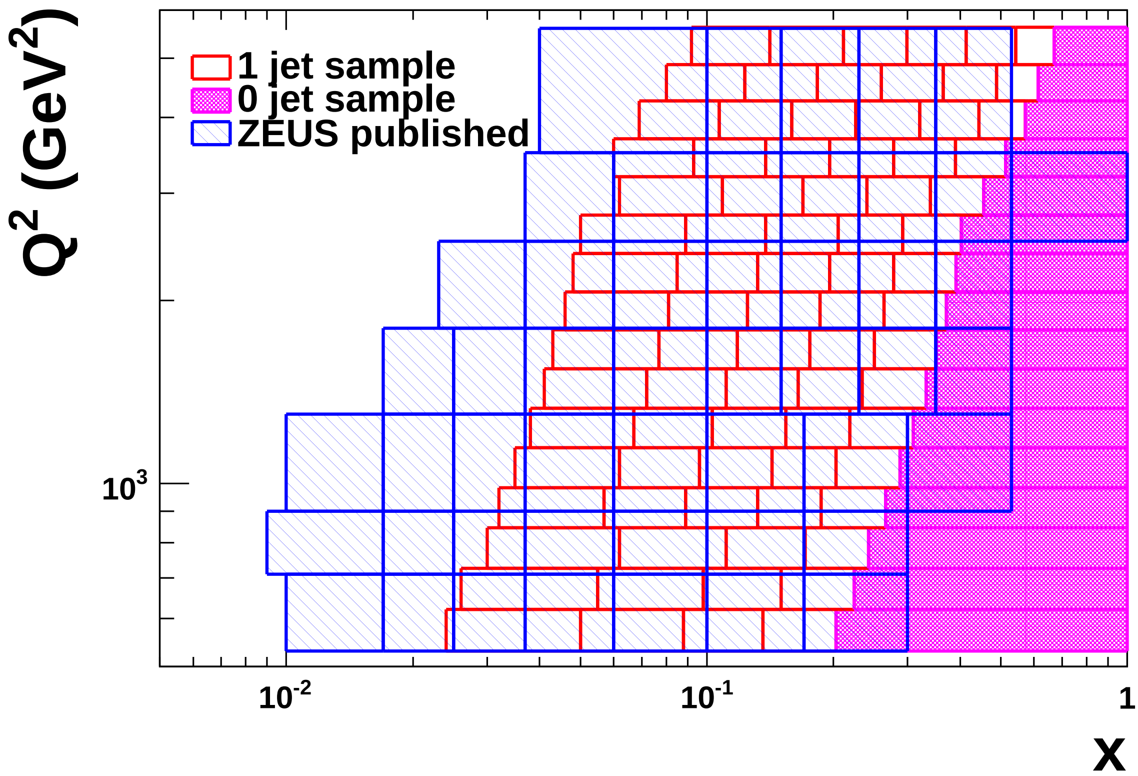

Figure 6: *Definition of the bins as used in this analysis. The magenta bins extending to $x = 1$ are for the zero jet events. The blue bins show the bin structure ZEUS published.*

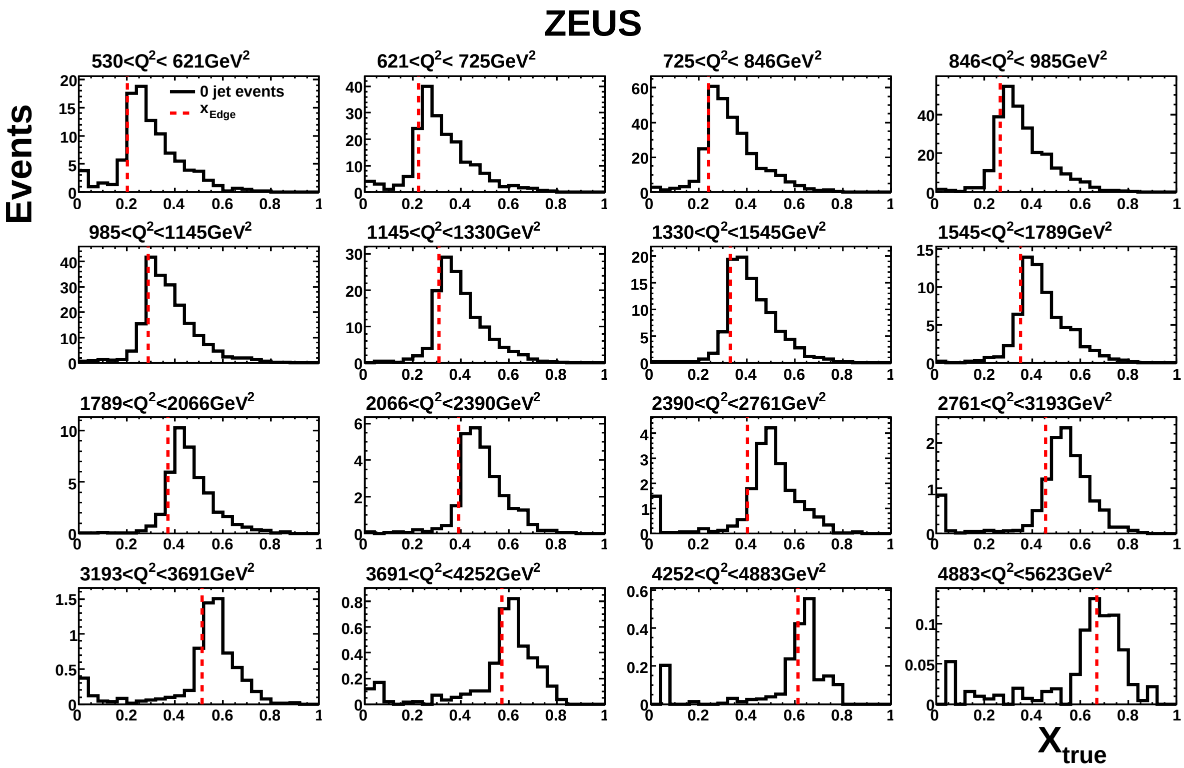

Figure 7: *The true x distribution from NC MC simulations for zero jet events in different Q^2 bins as indicated in the plots. The dashed lines represent the lower edge of the bins, x_{Edge}. The MC distributions are normalized to the luminosity of the data.*

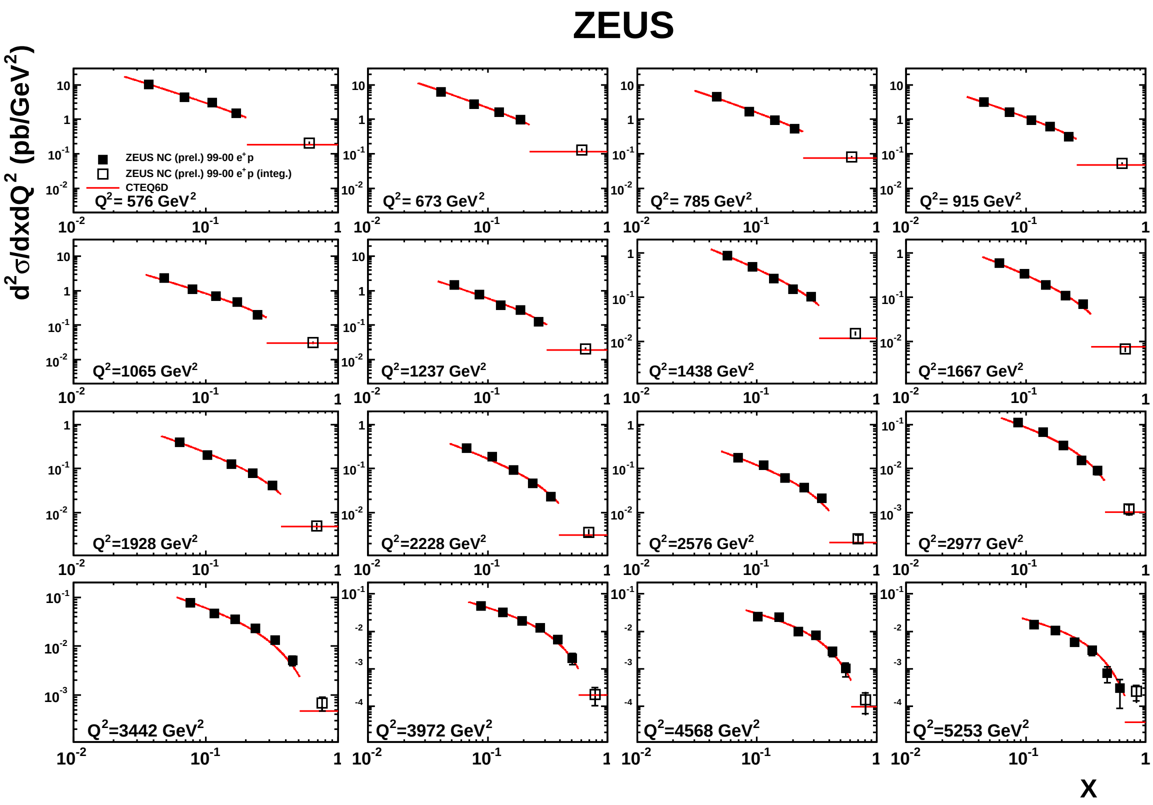

Figure 8: *The double differential cross section for e^+p NC scattering (solid squares) and the integral of the double differential cross section divided by the bin width (open squares) compared to the Standard Model expectations evaluated using CTEQ6D PDFs (lines). The inner error bars show the statistical uncertainty, while the outer ones show the statistical and systematic uncertainties added in quadrature.*

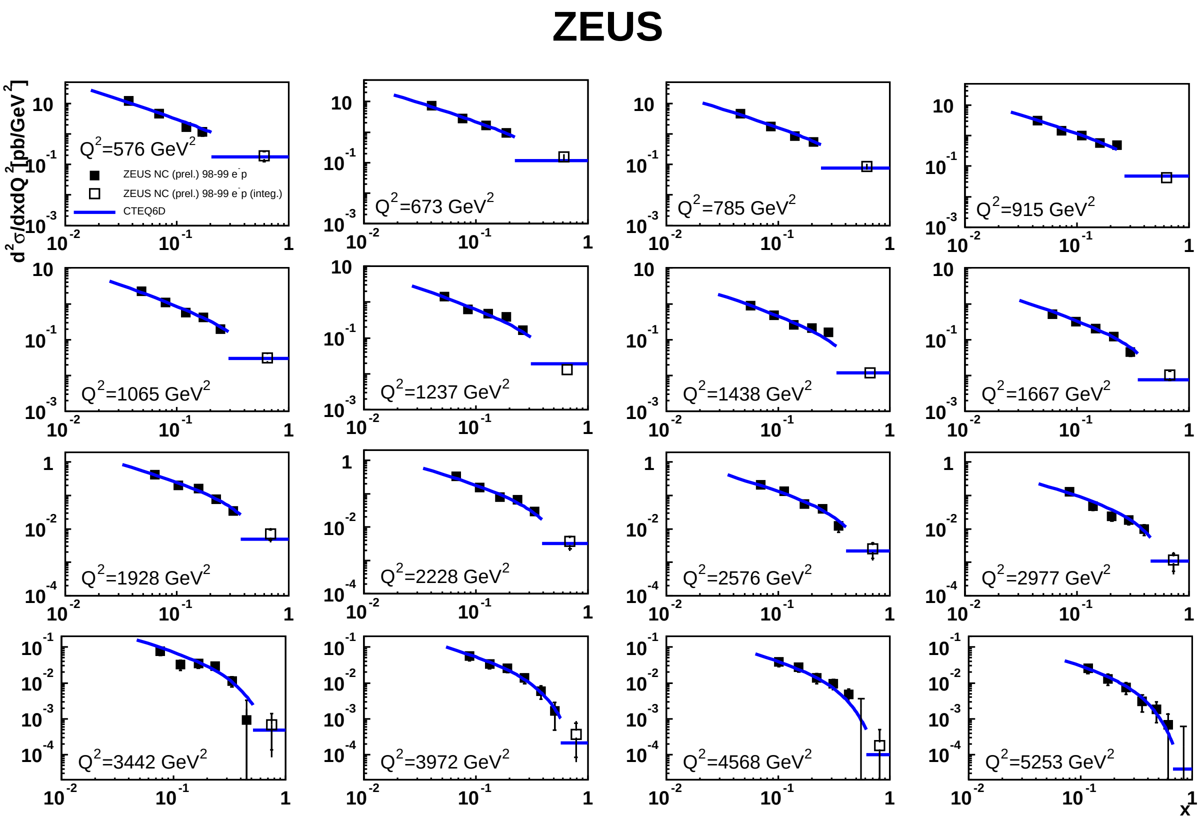

Figure 9: *The double differential cross section for e^-p NC scattering (solid squares) and the integral of the double differential cross section divided by the bin width (open squares) compared to the Standard Model expectations evaluated using CTEQ6D PDFs (lines). The inner error bars show the statistical uncertainty, while the outer ones show the statistical and systematic uncertainties added in quadrature.*

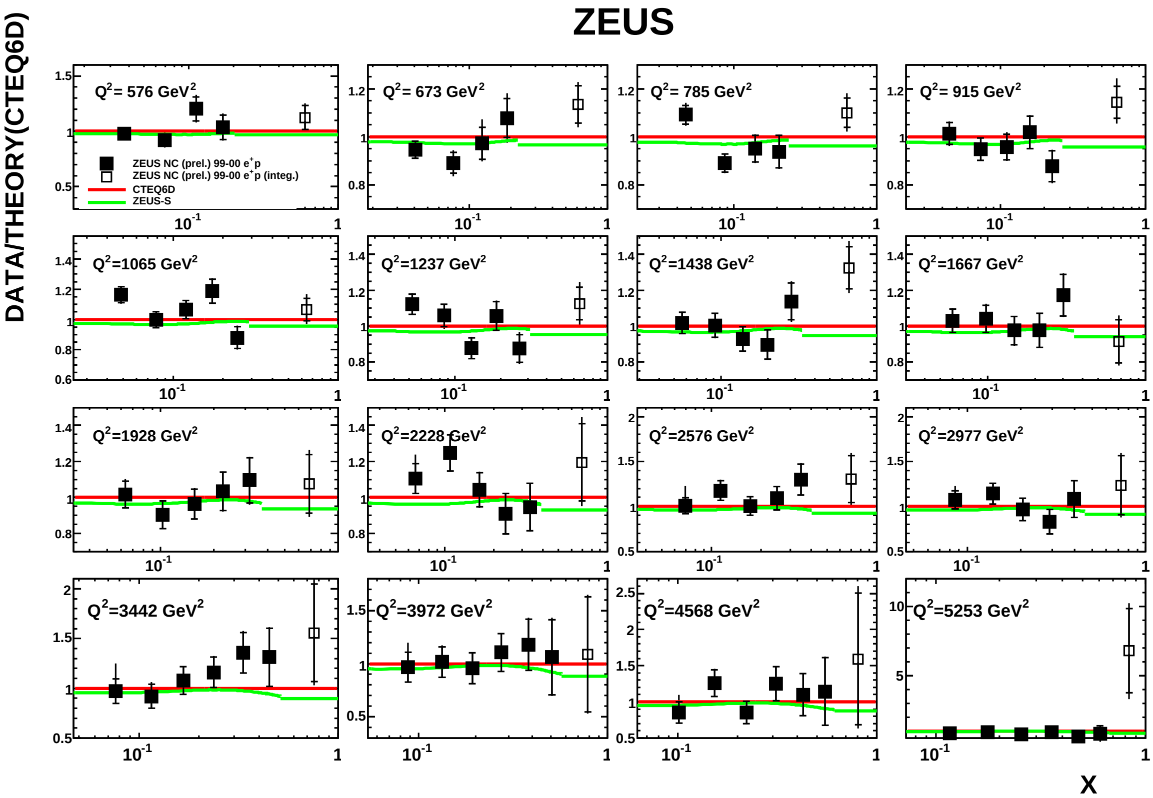

Figure 10: *Ratio of the double differential cross section for e^+p NC scattering (solid squares) and the integral of the double differential cross section divided by x bin width (open squares) to the Standard Model expectation evaluated using the CTEQ6D PDFs. The inner error bars show the statistical uncertainty, while the outer ones show the statistical and systematic uncertainties added in quadrature. The ratio of the expectations using the CTEQ6D PDFs to those using the ZEUS-S predictions is shown as the green (light) lines.*

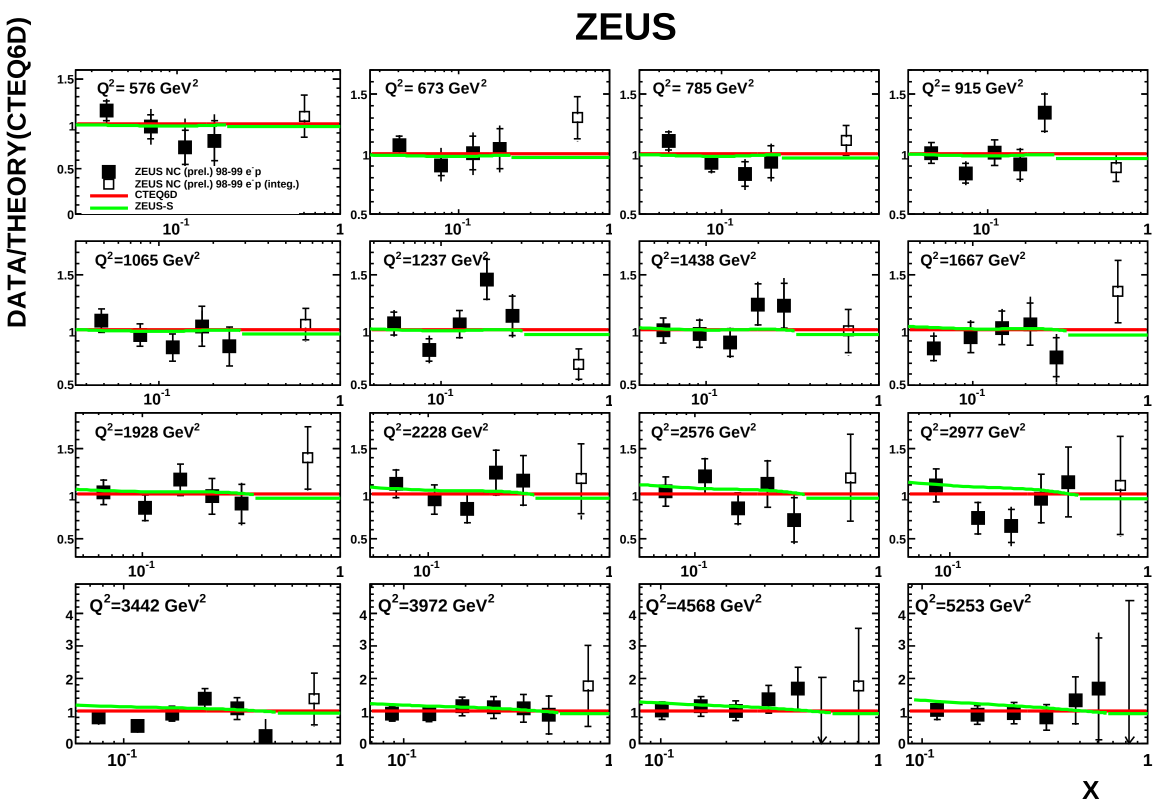

Figure 11: *Ratio of the double differential cross section for e^-p NC scattering (solid squares) and the integral of the double differential cross section divided by x bin width (open squares) to the Standard Model expectation evaluated using the CTEQ6D PDFs. The inner error bars show the statistical uncertainty, while the outer ones show the statistical and systematic uncertainties added in quadrature. The ratio of the expectations using the CTEQ6D PDFs to those using the ZEUS-S predictions is shown as the green (light) lines.*